Evaluation of Measurements of Particle Size and Sample Area from Optical Array Probes

A. V. KOROLEV, S. V. KUZNETSOV, YU E. MAKAROV AND V. S. NOVIKOV

Central Aerological Observatory, Dolgoprudny, USSR

(Manuscript received 19 July 1990, in final form 10 December 1990)

ABSTRACT

The technique of using shadow images of particles, obtained in coherent illumination to measure particle size, is analyzed. The theory of Fresnel diffraction for an opaque disc was used to analyze shadow images of transparent spherical particles. A comparison of theoretical calculations with laboratory results supports the application of this approach to optical array probes. It is shown that the shadow image size of spherical particles is essentially dependent on the distance from the object plane. In particular, for drops with diameters of less than 100 μm, the errors in size measurement from the PMS OAP-200X may reach 65%. These results agree well with laboratory calibrations that use monodisperse water droplets.

On the basis of calculated particle diffraction images, the shape of the sample area and its dependence on drop size were calculated. It was found that the sample area has a complicated sawtooth shape. Gaps oriented perpendicular to the axis of a laser beam occur in the sample area in the case of large droplets. Comparison of the sample area quoted by the manufacturer to the calculated one is considered.

1. Introduction

Optical array probes (OAPs) (Knollenberg 1970, 1976) have been used extensively over the last few years to study cloud-particle-size distributions and particle forms. Since their development (Knollenberg 1970) there have been a number of limited studies (Gayet 1976; Curry and Schemenauer 1979; Politovich 1982; MacIntante and Bartlett 1983; Gordon and Marwitz 1984; Hovenac et al. 1985; Baumgardner 1985, 1986, 1987; Hovenac 1986; Joe and List 1987) that have focused attention on the need for a clearer understanding of the principles underlying how OAP size measurements are obtained. In order to meet this need, a number of theoretical calculations in optics, laboratory studies of shadow images, and calibrations were performed.

Results of the theoretical and experimental study of diffraction images of an opaque disc and water droplets were reported by Hovenac et al. (1985) and Hirleman et al. (1988). Data on laboratory calibrations of OAPs were presented by Kuznetsov (1984), Baumgardner (1985, 1987), and Joe and List (1987). It was found that the measured particle size varies with the distance from an object plane. The dependence of the measured particle size on its distance from the object plane was found to be nonmonotonic and reliant on particle size. The obtained experimental dependencies have no clear theoretical explanation.

The principle of particle sizing in an OAP is based on obtaining measurements of particle shadow size with the help of a linear array of photodetectors. The optical system, using a He–Ne laser, produces bright-field illumination such that the particle images are dark shadows on a bright background. The particle shadows are projected on a linear array of photodiode elements. This detector array is used as a measuring grid to size the shadows of particles. When a particle traverses the laser beam near the object plane, its imaged shadow conceals a number of optical array elements. An element is considered concealed if loss of light is at least 50%. The size of the shadow is thus represented by an integral number of hidden array elements.

The depth of field for a given particle size is preset by utilizing a second 67% level detector. This second level is set to a darker threshold than the discriminator level used in sizing. Only one of the elements hidden at the 50% level is required to observe the 67% threshold for the particle to be within the depth of field. The selection of particles by a 67% level is used only in one-dimensional probes; this technique is not used in two-dimensional probes.

2. Theoretical study of spherical particle shadows

In general a particle shadow image is formed by diffracted, refracted, and absorbed components of light. The structure of the shadow image also depends on properties of the radiation such as coherence, monochromaticity, and laser beam divergence. One may find the exact solution of electromagnetic field scattering by a spherical particle using Mie theory (Deirmendjian 1969; Born and Wolf 1975). In practice, Mie calcu-

Corresponding author address: Dr. A. V. Korolev, Central Aerological Observatory, Dolgoprudny, USSR.

lations are rather laborious, especially in the case of large drops; i.e., the calculations take long run times on a computer and place excessive demands on memory. Because of computational difficulties, we shall use some simplifications.

First, spherical water drops in visible light are known to be short-focus collecting lenses with a focal length of approximately equal to their radii. We can neglect the refracted component of light and consider water drops to be opaque spheres in the analysis of their diffraction image at a distance of more than ten radii. Thus, the shadow images of water drops will be defined mainly by the diffracted component.

The second simplification consists of using diffraction by an opaque plane disc to represent the diffraction by spherical particles. In OAPs, drop sizes ($D > 20$ μm) are much larger than the wavelength of light ($\lambda = 0.6328$ μm), so the Huygens–Fresnel approximation can be used for calculation of the light intensity in the diffraction image.

Suppose a plane wave is incident perpendicularly on an opaque disc with radius R (Fig. 1). Following Born and Wolf (1975) the amplitude of a diffracted wave at point Q may be represented as

$$U(Q) = U_a(Q) + U_b(Q) \tag{1}$$

where

$$U_a(Q) = \begin{cases} \exp(iK\mathbf{kg}) & \text{if point Q is outside the geometrical shadow} \\ 0 & \text{if point Q is within the geometrical shadow} \end{cases} \tag{2}$$

where $\mathbf{k} = \mathbf{K}/|\mathbf{K}|$ is a unit vector in the direction of plane wave propagation, $K = 2\pi/\lambda$ is the wavenumber, and $\mathbf{g}$ is the radius vector of point Q. Thus,

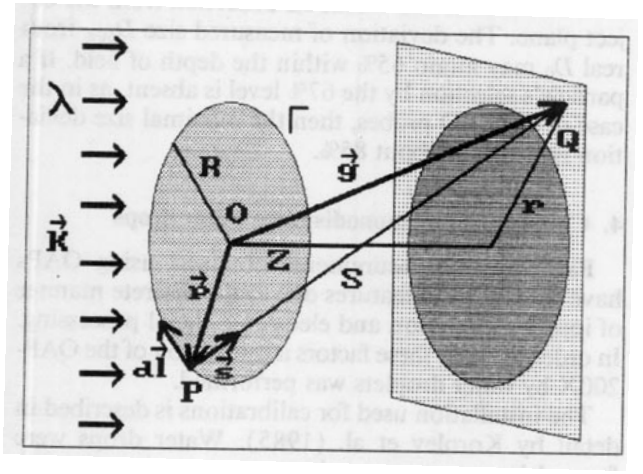

FIG. 1. An opaque disc illuminated by a plane wave creates a diffraction pattern at point Q.

$$U_b(Q) = \frac{1}{4\pi}\oint_\Gamma \exp(i\mathbf{kp})\frac{\exp(iKS)(\mathbf{s}\times\mathbf{k})}{S(1-\mathbf{sk})}\,d\mathbf{l} \tag{3}$$

where $\mathbf{p}$ is the radius vector of point P on contour Γ, $d\mathbf{l}$ is the differential element of length along contour Γ, S is the distance between points P and Q, and $\mathbf{s}$ is the unit vector on the PQ direction (Fig. 1).

Integration is carried out along contour Γ, the boundary of the geometrical shadow.

Let the origin of coordinates (point O) be placed in the center of the disc. Then (2) may be written as

$$U_a(Q) = \begin{cases} \exp(iKZ) & \text{if } r > R \\ 0 & \text{if } r \leqslant R \end{cases} \tag{4}$$

where r is the distance between point Q and the center of the geometrical shadow and Z is the distance between the disc and the center of the image.

Substituting in (3) integration along the contour for integration with respect to angles we obtain:

$$U_b(Q) = -\frac{1}{4\pi}\int_0^{2\pi}\frac{\exp(iKS)}{Z}\frac{R^2 - Rr\cos\alpha}{S - Z}\,d\alpha \tag{5}$$

where $S = (R^2 + Z^2 + r^2 - 2Rr\cos\alpha)^{1/2}$.

Let us expand S in a power series $(R^2 + r^2 - 2Rr \times \cos\alpha)/Z^2$ and keep only two first terms (the Fresnel approximation). Then (5) becomes

$$U_b(Q) = -\frac{\exp(iKZ)}{2\pi}\int_0^{2\pi}\exp\left[\frac{i\pi}{Z_d}(1 + \xi^2 - 2\xi\cos\alpha)\right]\frac{1 - \xi\cos\alpha}{1 + \xi^2 - 2\xi\cos\alpha}\,d\alpha \tag{6}$$

where $\xi = r/R$ is the normalized radial coordinate on the object plane and $Z_d = Z\lambda/R^2$ is the dimensionless diffraction parameter.

Using (1), (4), and (6) we calculate the intensity of the diffraction image as

$$I(\xi) = |U(\xi)|^2. \tag{7}$$

From (6) and (7) it follows that if ξ is fixed, the increase of disc size will change the scale of the image but will not distort its form: i.e., if ξ is constant, the form of the shadow image depends only on $|Z_d|$.

Note that the above approach is true for $|Z_d| > 200\ \lambda^2/\pi R^2$ (Papoulis 1968).

In the above calculations we do not take into account the influence of the aperture of imaging optics. Consideration of the parameters of imaging optics will unjustifiably complicate the final result. Our preliminary analysis has shown that neglect of the OAP aperture has only a slight influence on the particle diffraction image. One may find a more detailed analysis of the

influence of imaging optics on the disc diffraction image in Schaub et al. (1990).

3. Experimental study of diffraction images of glass beads

To study the assumption that shadow images of spherical particles can be represented by the diffraction pattern of an opaque plane disc, described by (7), an experimental study of diffraction images of transparent glass beads was performed. The method used was similar to that described by Gayet (1976). A glass bead was placed on a thin (0.1 mm) parallel-plane glass plate, fixed on a three-coordinate micrometrical stage. The glass bead was placed in the center of the laser beam with the help of a micrometrical feed.

In order to diminish the influence of the glass plate on the diffraction image, the experimental plant was mounted so that the laser beam was incident on the bead after passing through the glass plate. Since the glass plate is plane-parallel, the distortions in the wave front incident on the glass bead are negligible. The distortions introduced by the glass plate in the diffraction image of the glass bead are mainly defined by double reflections from the outer or inner surface of the bead, and afterwards, from the plate itself. When the angle of incidence is close to 90° (namely, these beams get into the objective aperture and form the diffraction image), the glass surface reflects 2%–5% of the incident light. Thus, the sum influence of the plate on the intensity distribution of the diffraction image must not exceed 1%.

The diffraction pattern formed by the OAP's optics was projected on the screen fixed on a two-coordinate plotter. The light intensity was measured using a photodiode fixed on the head of the plotter. The head movement and the process of photodiode measurement were computer controlled. The experimental configuration was modeled using the optics and the illumination system of the OAP-200X.

The scanning of a diffraction pattern was carried out along seven radial directions. The scanning step was 1 mm, and the accuracy of displacement was 0.25 mm. The dimensions of the projected geometrical shadows ranged from 80 to 100 mm. During data processing the light intensity $I(R)$ was normalized by the background intensity $I_0(R)$ measured in the absence of particles and then averaged over all radial directions. This procedure made it possible to diminish the optical pollution effect and to account for the intensity variations in the laser beam. About 70 diffraction images for glass beads of size 43, 103, 107, 115, and 238 μm were examined utilizing the above technique.

Figures 2a–d show a comparison of the experimental data with the theoretical calculations performed using (6) and (7) for various displacements from the object plane. As seen in Fig. 2, the experimental results agree well with theoretical calculations. We compared various diffraction images of glass beads with calculated ones and found the results to be similar to those in Fig. 2. However, some discrepancies are observed in the region of the central peak (Poisson spot) when $|Z_d| < 1.5$. The differences are caused by neglecting the component of light refracted by the glass bead, as well as the aperture and other parameters of the imaging optics in the calculation of a diffraction pattern.

Except for the central zone of the diffraction image, the discrepancies between theoretical and experimental data do not exceed 10%. This allows us to utilize the approach of Fresnel diffraction in the analysis of the accuracy of the OAP.

It was mentioned earlier that in the OAP, a 50% threshold level is used for particle image sizing. We denote the shadow image size as $D_{\%}$. Figure 3 presents the comparison of theoretical and experimental normalized sizes $D_{\%}/D_0$ versus parameter Z_d; here D_0 is a measured bead geometrical diameter. Values of $D_{\%}/D_0(Z)$ were computed for 50% (curve 1) and 67% (curve 2) shadow intensity levels.

The upper part of curve 1 corresponds to the drop size to be registered by the probe $D_{50\%}$ (see Fig. 2d). The lower part of this curve corresponds to the size of a central peak (Poisson spot) $P_{50\%}$ at 50% shadow level. One can often observe this bright spot in the center of a shadow image of drops in the two-dimensional OAP data. The lower part of curve 1 shows the increase of $P_{50\%}$ with the increase of Z_d. Curve 2 represents the 67% shadow level of a diffraction image. This curve shows that when $|Z_d| > |Z_{d\max}| = 4.8$, the diffraction image has no zones where light intensity is less than 67% shadow level. This means that if $|Z_d| > |Z_{d\max}|$, the drop will be rejected by the probe electronics. This is true only for the one-dimensional OAP.

The best agreement with experimental results is obtained for beads larger than 40 μm. The above curve (Fig. 3) allows us to evaluate the effect of the distortion of the measured size versus its deflection from the object plane. The deviation of measured size $D_{50\%}$ from real D_0 may attain 65% within the depth of field. If a particle's selection by the 67% level is absent, as in the case of OAP-2D probes, then the maximal size deviation may attain about 85%.

4. Calibrations by monodisperse water drops

Particle-size measurements obtained using OAPs have some typical features due to the discrete manner of image registration and electronic signal processing. In order to study these factors a calibration of the OAP-200X by water droplets was performed.

The installation used for calibrations is described in detail by Korolev et al. (1985). Water drops were formed by a generator with a vibrating needle. The generator used made it possible to obtain monodisperse

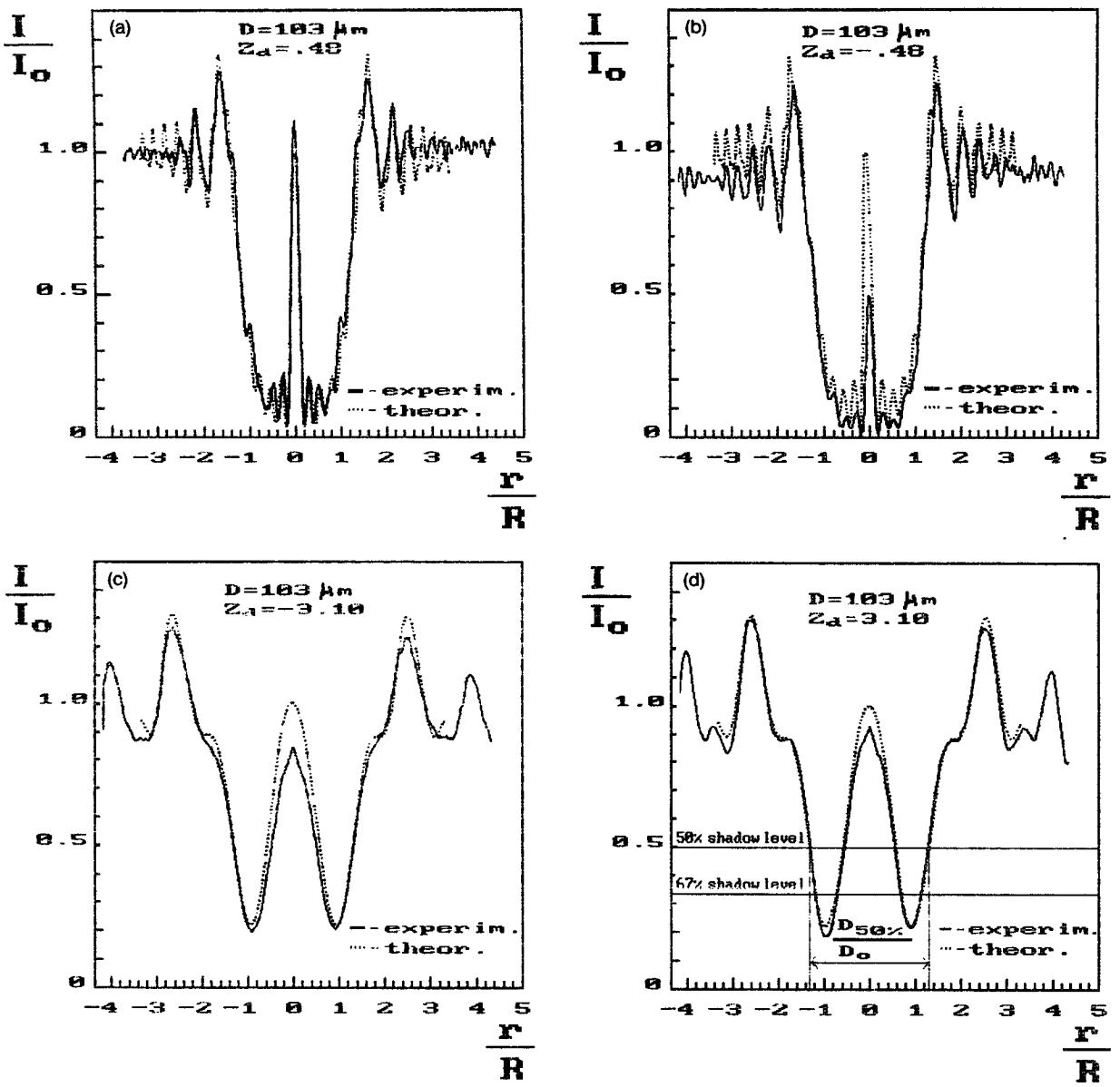

FIG. 2. Comparison of light intensity distributions of diffraction images of a 103-μm glass bead measured experimentally and calculated from (7) for various values of dimensionless parameter $Z_d = Z\lambda/R^2$.

drops with a mean-square error in diameter of not more than 2%. Drop velocity was in the range of 2–10 m s^{-1}. The drops were sized by microphotographs obtained in transmitted stroboscope light (Fig. 4a). Another method involves measuring the glare distance that appears when drops are illuminated by a laser beam (Fig. 4b). Glare distance D_s is related to drop-size D_0 by the following formula:

$$D_0 = \frac{D_s}{2}\left\{\frac{n\cos(\gamma/2)}{[1+n^2-2n\cos(\gamma/2)]^{1/2}} - \sin(\gamma/2)\right\} \quad (8)$$

where γ is an angle between the optical axes of the microscope and a laser beam, and n is the refractive index of water. Errors of drop-size measurements did not exceed 2%–3%.

Drop sizing by measuring the glare distance is more precise than that obtained using microphotography. Two glare streaks shown in Fig. 4a appear only when $100° < \gamma < 180°$. The maximum precision of drop sizing is obtained when $\gamma = 120°$–$130°$. The use of a microscope to observe glare makes it possible to control operatively the size stability of generated drops, the drop jet divergence, and the position of the drops in a

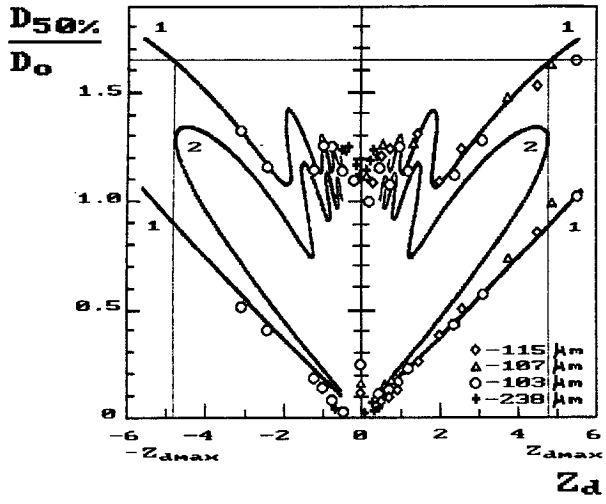

FIG. 3. Experimental 50% level diffraction sizes of glass beads. Theoretical 50% level (1) and 67% level (2).

laser beam. The deflection of drops from the axis of a jet did not exceed 20–50 μm in the above calibration.

Figure 5a shows the registered size of drops as a function of their displacement Z along the laser beam. Usually at a fixed position of the drop generator in the vicinity of the object, plane drops are registered in one channel; but at the peripheral part of the laser beam, drops are registered in two or three channels simultaneously. Therefore, every point on the plot is a mean registered size obtained by averaging over 600–700 drop registrations.

One may distinctly observe (Fig. 5a) an increase in measured size as the distance from the central part of the beam increases. The above picture shows that the mean registered size for a drop with a definite size may vary in the range of five channels. Similar results were obtained earlier by Kuznetsov (1984), Baumgardner (1985, 1987), and Joe and List (1987).

During calibration it was noted that when drops leave the depth of field, the number of drops to be registered does not diminish sharply, as was previously expected based on the work of Hovenac et al. (1985), but smoothly. Figure 5b shows the relative number of registrations $\delta = N_r/N_0$ versus displacement along the laser beam for a 98-μm drop; here N_0 is the number of drops that passed through the laser beam, and N_r is the number of registered drops. For a given drop size the interval where drops register occupies about 49 mm. The zone where $\delta > 0.5$ is equal approximately to 34 mm. On the other hand, the theoretical value of the depth of field for a 98-μm droplet equals 36 mm (see section 5). We find that the distance of removed depth-of-field registrations strongly depends on drop size. The effect of removed depth-of-field drop registrations leads to additional distortion of the registered particle-size distribution, because $D_{50\%}$ monotonically increases when $|Z_d|$ increases (for $|Z_d| > 1.9$) (see Fig. 3).

The effect of removed depth-of-field drop registrations is important only for those drops whose depth of field does not exceed the size of the probe's aspirator Z_{asp} (the distance between the OAP probe arms). In particular, for the OAP-200X, the sizes of these drops are equal to 126 μm. For the drops with $D > 126$ μm, the depth of field is constant and equal to $Z_{asp} = 61$ mm.

The comparison of theoretical calculations with calibrations is shown in Fig. 6. The displacement from the object plane Z was converted into the dimensionless coordinate Z_d. The disagreement between the experimental points and our calculation is related both to the discrete technique of registration and to the aspects mentioned in section 2.

5. Sample area

In a one-dimensional OAP the sample area calculation utilizes a number of criteria for particle selection

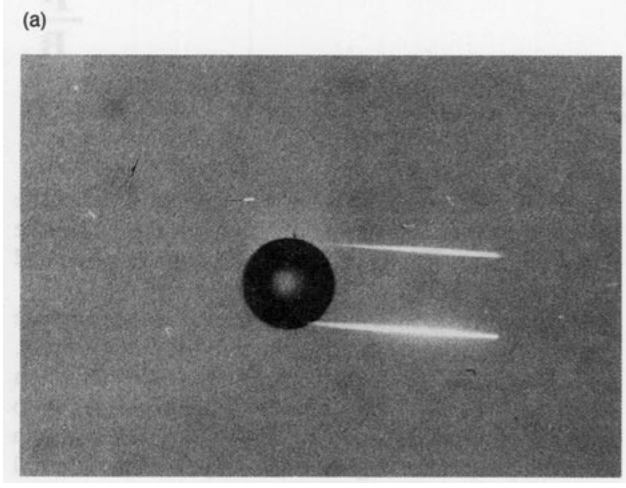

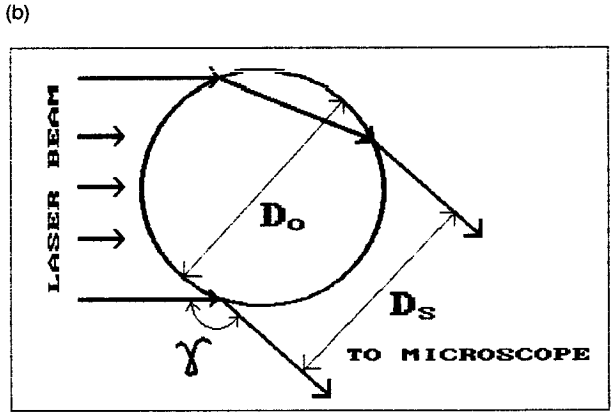

FIG. 4. (a) Microphotograph of drop obtained in transmitted stroboscopic illumination. The glares (two bright lines) appears when the drop passes through the laser beam of the probe. (b) Schematic of glare formation on a drop.

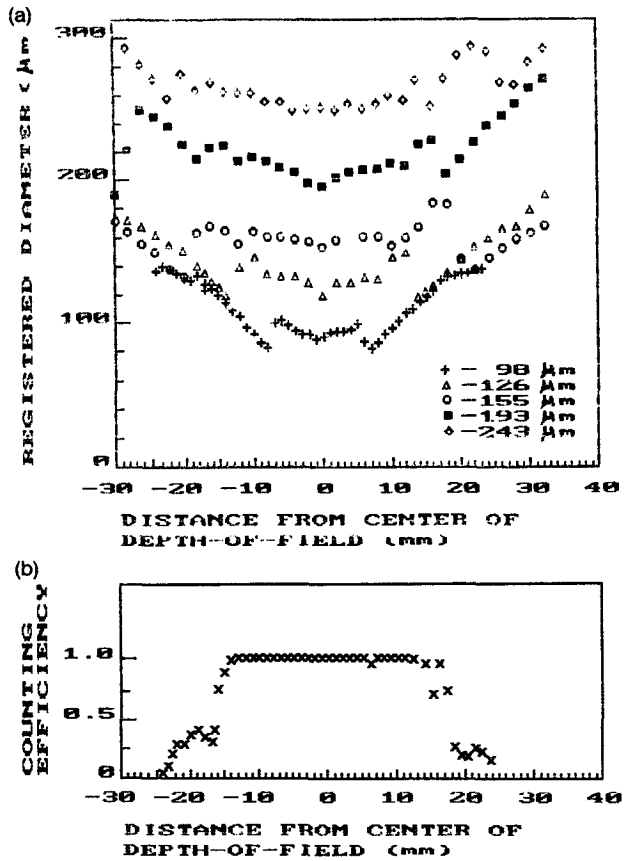

FIG. 5. (a) OAP-200X registered size of drops versus displacement along the laser beam. (b) Relative number of registrations $\delta = N_r/N_0$ versus displacement along the laser beam for 98-μm drop.

and is therefore a rather complicated procedure. In one-dimensional probes the sample area is formed by rejection of particles using three criteria. First, particles are not registered unless at least one element is shadowed more than 67%. Second, particles that shadow one of two edge photodiodes are not registered. Third, the one-dimensional OAP used in this study sizes drops in 15 discrete channels, where the size of channel N corresponds to the products of the N diodes shadowed by the resolution of the probe. Drops that are larger than the 15th channel will be rejected.[1]

The first condition is used to form the sample area along the laser beam axis. The rejection of particles by the 67% level is used in order to avoid large errors in sizing when the displacement from the object plane is large.

Analysis of the diffraction images (sections 2, 3) shows that light shadow intensity within the particle image decreases when displacement Z_d increases. Using Fig. 3, one may find that when $|Z_d| > |Z_{d\max}| = 4.8$ the diffraction image has no zones where light intensity is less than the 67% shadow level. Recall that due to the conformity of the diffraction image formation, $Z_{d\max}$ is constant for all spherical particles.

The effective depth-of-field Z_s^0 for a drop with diameter D according to Knollenberg (1970), is given by

$$Z_s^0 = A\frac{D^2}{4\lambda}. \tag{9}$$

In our case the coefficient A is equal to $2Z_{d\max}$, and therefore $A = 9.60$.

For drops $D > 126$ μm, the depth of field exceeds the size of the probe's aspirator Z_{asp}, so the depth of field will be

$$Z_s = \min(Z_s^0; Z_{asp}). \tag{10}$$

The second condition forms the width of the sample area. When a laser beam is parallel, the sample area width equals

$$L_s = \frac{w}{m}(h-1) - D_{50\%}(Z) \tag{11}$$

where m is the optical magnification, w is the distance between the diode centers of the photodiode line, and h is the number of elements in the photodiode line (for the OAP-200X, $h = 24$) (Fig. 7).

The first term of (11) characterizes the width of the sample area, which is defined by the size of a diode line $w(h-1)$ transformed by imaging optics with magnification m to the domain of a sample volume. The second term is conditioned by the diminishing of the sample area width when the drop image covers one of the two edge photodiodes.

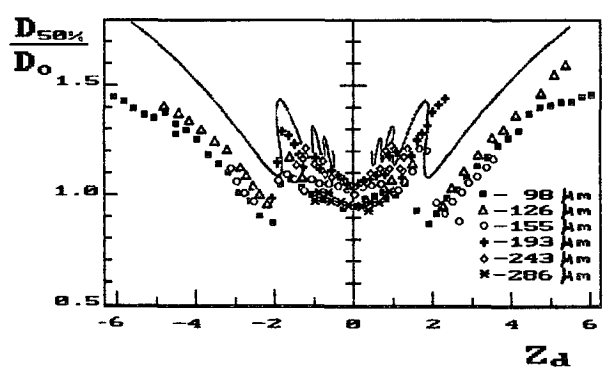

FIG. 6. Comparison of OAP-200X registered normalized droplet sizes versus dimensionless displacement Z_d with theoretical calculations.

[1] This criterion is not used in the OAP-260X.

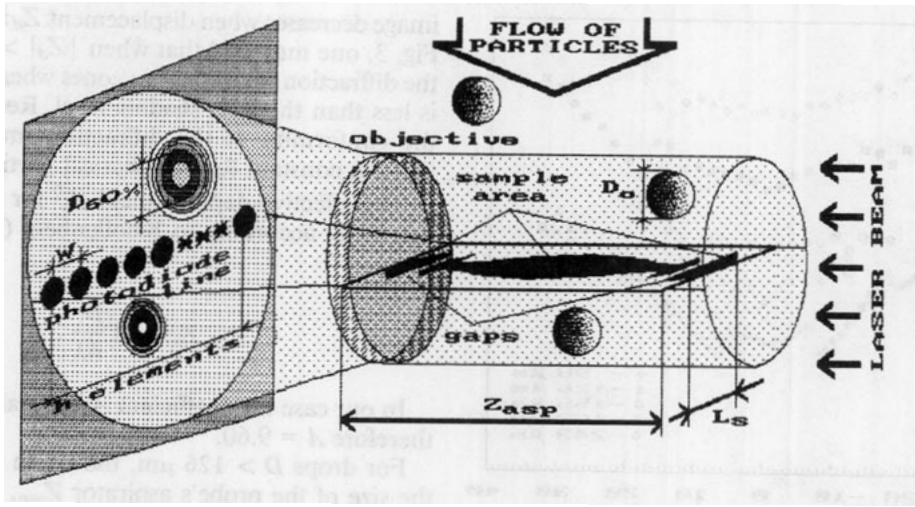

FIG. 7. Sample area of one-dimensional OAPs.

From (11) it follows that the sample area is sawtooth-shaped because $D_{50\%}$ is an oscillating function (see Figs. 3, 5), and in this it differs from the ones given by Knollenberg (1970) and by Hovenac et al. (1985).

The gaps in the sample area are formed in accordance with the third criterion. As the distance between the particle and the object plane increases, when $|Z_d| < 1.9$, the measured drop diameter oscillates (Fig. 3). If at some distance $D_{50\%}$ becomes more than $D_{\max}$, i.e., the shadow image covers more than 15 diodes, the particle will be rejected. This results in the appearance of the gap (Fig. 7). With the further increase of Z, $D_{50\%}$ may become less than $D_{\max}$; then the particle is registered again. Such gaps are typical of large drops. In particular, in the case of the OAP-200X the gaps appear for drops with $D_0 > 250$ μm. Gaps are absent in the case of the probes without rejection of particles by maximum size (OAP-260X, two-dimensional OAPs).

Taking into account the limitations on maximal registered size $D_{\max}$ the sample area width is expressed as

$$L_s(Z) = \begin{cases} \dfrac{w}{t}(h-1) - D_{50\%}(Z) & \text{if } D_{50\%}(Z) < D_{\max} \\ 0 & \text{if } D_{50\%}(Z) \geqslant D_{\max}. \end{cases} \quad (12)$$

The calculated sample area shape for different drops is shown in Fig. 8. These plots illustrate the sawtooth shape of the sample area and the presence of gaps. The sawtooth shape and gaps in the sample area were distinctly observed during OAP-200X water drop calibrations. These gaps are associated with the manner of particle selection and are typical for large drops (D

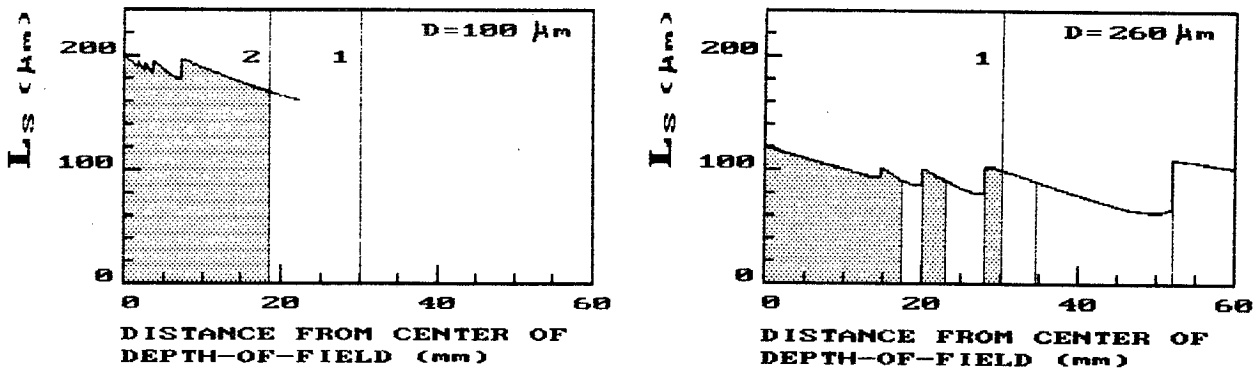

FIG. 8. Calculated form of the sample area of the OAP-200X for spherical particles. Due to symmetry a quarter of the sample area is shown. Section-lined areas are the zones where the particle is registered by the probe. Vertical lines denote the probe aspirator bound (1) and 67% level bound of registration (2). (a) $D = 100$ μm. The sample area is sawtooth-shaped. (b) $D = 260$ μm. The gaps appeared in the sample area.

> 250 μm). Note that these gaps are perpendicular to the laser beam axis. Another type of gap was observed during calibrations for small drops ($D < 30$ μm). These gaps are parallel to the laser beam axis and arise due to the discrete character of the photodiode array.

The sample area was calculated as

$$S(D) = \int_0^{Z_s(D)} L_s(Z)dZ. \qquad (13)$$

Figure 9 compares $S(D)$ calculated using (13) to that provided by the manufacturer. When $D < 120$ μm the discrepancy is due to the neglect of the dependence of the particle shadow image on the displacement along the laser beam. When $D > 250$ μm the disagreement is due to the neglect of gaps in the sample area.

6. Conclusion

One of the main conclusions drawn from our work is that shadow images of transparent spherical particles obtained with coherent light are accurately described by the Fresnel diffraction for an opaque disc. This allows the use of Fresnel diffraction in the analysis of shadow-technique probes.

The above theoretical and experimental study shows, in the case of one-dimensional OAPs, that

- registered drop size is essentially dependent on the displacement from the object plane. In particular, for the OAP-200X, size errors may reach 65%. For OAP-2D probes, size errors for small particles may reach about 85%.
- The sample area has a complicated sawtooth shape and is not rectangular as was previously believed. In the sample area there are gaps oriented perpendicular to laser beam axis for large drops ($D > 250$ μm in the case of the OAP-200X) and parallel gaps for small ones.

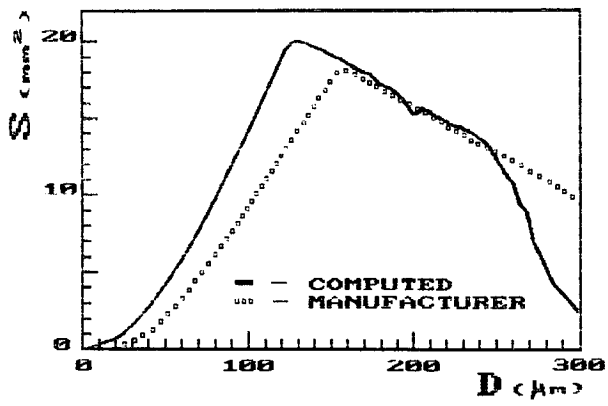

FIG. 9. Comparison of calculated and manufacturer-supplied functions of a square of the sample area versus the size of spherical particle.

Note that in the calculation of the sample area errors arising from electronic signal processing and errors arising from the discrete manner of image registration were neglected. In fact, when airspeed is close to or over 100 m s^{-1}, distortion of the output signal takes place. This results in a decrease in the measured particle size and, consequently, in the variations in the sample area. The influence of the airspeed on the depth of field of the one-dimensional OAP was reported by Baumgardner (1987). It was shown that an increase in the airspeed causes a decrease in the depth of field. On the other hand, it follows from (11) that the decrease of the measured particle size at a higher speed results in an increase of the width of the sample area and in a diminishment or disappearance of gaps. These two effects will compensate for each other to some extent. The influence of airspeed on the sample area needs further detailed experimental and theoretical study.

Some other aspects of the electronics of the OAP were discussed by Kuznetsov (1984), Baumgardner (1987), and Baumgardner et al. (1986). It was shown that the electronics in the OAP result in a number of errors in particle sizing and particle undercounting.

The treatment of all errors using direct particle calibrations is extremely difficult or even impossible, so it seems reasonable to consider the effect of various errors using a numerical simulation.

When one attempts to measure particles of an arbitrary shape, the complexity of the problem of reconstructing the particle-size distribution increases appreciably. Even in the presence of a priori information about particle shapes and space orientation the problem remains extremely complicated. One should proceed with care when interpreting microstructural data obtained in solid or mixed clouds with one-dimensional OAPs.

Acknowledgments. The present work was completed in the scope of program on cloud investigations in central Aerological Observatory in the USSR.

REFERENCES

Baumgardner D., 1985: Particle size calibrations of two optical array probes. Newsletter on Developments of Airborne Cloud Physics Instruments, NCAR, Boulder, 1–3.

——, 1987: Corrections for the response times of particle measuring probes. Sixth Symp. Meteorological Observation and Instrumentation, New Orleans, Amer. Meteor. Soc. 148–151.

——, J. E. Dye and W. A. Cooper, 1986: The effects of measurement uncertainties on the analysis of cloud particle data. *Preprints Conf. on Cloud Physics,* Snowmass, CO, Amer. Meteor. Soc., 313–316.

Born, M., and E. Wolf, 1975: *Principles of Optics.* 5th ed., Pergamon.

Curry, M. J., and R. S. Schemenauer, 1979: The small-particle response of an optical array precipitation probe. *J. Appl. Meteor.,* **18,** 816–821.

Deirmendjian, D., 1969: *Electromagnetic Scattering on the Spherical Polydispersion.* Elsevier, 290 pp.

Gayet, J. F., 1976: Physique de la mesure du spectre dimensionnel

de gouttes de nuages au moyen des capteurs de Knollenberg. Thèse de 3e Cycle (1re Partie) Recherche de l'Université de Clermont-Ferrand, 57 pp. (in French).

Gordon, G. L., and J. D. Marwitz, 1984: An airborne comparison of three PMS probes. *J. Atmos. Oceanic Technol.*, **1,** 22–27.

Hirleman, E. D., D. J. Holve and E. A. Hovenac, 1988: Calibration of single particle sizing velocimeters using photomask reticles. *Proc. Fourth International Symp. on Applications of Laser Anemometry of Fluid Mechanics,* Lisbon, LADOAN, 1–5.

Hovenac, E. A., E. D. Hirleman and R. F. Ide, 1985: Calibration and sample volume characterization of PMS optical array probes. *International Conf. on Liquid Atomization and Spray Systems,* The Institute of Energy, London.

——, 1986: Use of rotating reticles for calibration of single particle counters. Laser Institute of America, **58,** 129–134.

Joe, P., and R. List, 1987: Testing and performance of two-dimensional optical array spectrometers with greyscale. *J. Atmos. Oceanic Technol.*, **4,** 139–150.

Knollenberg, R. G., 1970: The optical array: An alternative to scattering and extinction for airborne particle size determination. *J. Appl. Meteor.*, **9,** 86–103.

——, 1976: Three new instruments for cloud physics measurements: The 2D spectrometer probe, the forward scattering spectrometer probe, and the active scattering spectrometer probe. *Preprints the International Conf. on Cloud Physics,* Boulder, Amer. Meteor. Soc., 554–561.

Korolev, A. V., Yu. E. Makarov and V. S. Novikov, 1985: On the calibrations of photoelectric cloud droplet spectrometer FSSP-100. *Tr. CAO,* **158,** 43–49. (in Russian).

Kuznetsov, S. V., 1984: Study of cloud droplet spectrometer OAP-200X. Graduater Paper, Moscow Physical Technical Institution, Dolgoprudny, 78 pp. (in Russian).

MacIntante, M., and B. M. Bartlett, 1983: Responce of the OAP-2D-C to small drops. Newsletter on the Development of Airborne Cloud Physics Instruments, NCAR, Boulder, 1–3.

Papoulis, A., 1968: *System and Transforms with Application in Optics.* McGraw-Hill,

Politovich, M. K., 1982: Calibration and comparison of OAP's using oil coated slides. *Cloud Particle Measurement Symposium: Summaries and Abstracts,* D. Baumgardner and J. Dye, Eds., NCAR Tech. Note/TN-199+PROC., 69–72.

Schaub, S. A., D. R. Alexander and J. P. Barton, 1990: Modeling of a coherent imaging system. *Proc. Second International Congress on Optical Particle Sizing,* Tempe, Arizona State University, 239–250.